

European Journal of Applied Mathematics

<http://journals.cambridge.org/EJM>

Additional services for ***European Journal of Applied Mathematics***:

Email alerts: [Click here](#)

Subscriptions: [Click here](#)

Commercial reprints: [Click here](#)

Terms of use : [Click here](#)



The maximum voltage drop in an on-chip power distribution network: analysis of square, triangular and hexagonal power pad arrangements

TOM CARROLL and JOAQUIM ORTEGA-CERDÀ

European Journal of Applied Mathematics / *FirstView* Article / June 2014, pp 1 - 21
DOI: 10.1017/S0956792514000114, Published online: 23 April 2014

Link to this article: http://journals.cambridge.org/abstract_S0956792514000114

How to cite this article:

TOM CARROLL and JOAQUIM ORTEGA-CERDÀ The maximum voltage drop in an on-chip power distribution network: analysis of square, triangular and hexagonal power pad arrangements .
European Journal of Applied Mathematics, Available on CJO 2014 doi:10.1017/S0956792514000114

Request Permissions : [Click here](#)

The maximum voltage drop in an on-chip power distribution network: analysis of square, triangular and hexagonal power pad arrangements

TOM CARROLL¹ and JOAQUIM ORTEGA-CERDÀ²

¹ *Department of Mathematics, University College Cork, Cork, Ireland*
email: t.carroll@ucc.ie

² *Departament de Matemàtica Aplicada i Anàlisi, Universitat de Barcelona,*
Gran Via 585, 08007 Barcelona, Spain
email: jortega@ub.edu

(Received 9 July 2013; revised 13 March 2014; accepted 17 March 2014)

A mathematical model of the voltage drop which arises in on-chip power distribution networks is used to compare the maximum voltage drop in the case of different geometric arrangements of the pads supplying power to the chip. These include the square or Manhattan power pad arrangement, which currently predominates, as well as equilateral triangular and hexagonal arrangements. In agreement with the findings in the literature and with physical and SPICE models, the equilateral triangular power pad arrangement is found to minimize the maximum voltage drop. This headline finding is a consequence of relatively simple formulas for the voltage drop, with explicit error bounds, which are established using complex analysis techniques, and elliptic functions in particular.

Key words: Mathematical problems of computer architecture; Elliptic functions and integrals; Poisson's equation

1 Introduction

Control of the maximum voltage drop between power distribution pads is a factor of increasing importance in the design of the power distribution network (PDN) of modern IC computer chips. The voltage drop between power pads depends on both the current flowing in the power mesh between the pads and the electrical resistance in the power mesh. Technological advances lead to higher current densities on the microprocessor, which in turn lead to higher voltage drops. At the same time, lower supply voltages imply lower tolerable voltage drops. Thus, as technology advances, the necessity to eliminate large voltage drops at the design stage becomes of increasing importance. The physical layout of a computer chip and the interaction between the chip and its PDN are described in detail by Shakeri and Meindl [9] in the context of both wire-bond and flip-chip PDN design. They focus on a dominant paradigm in which the power pads and the power mesh are arranged in a square grid, which is known as the Manhattan architecture; they derive the equations governing the voltage drop and provide the leading terms of the solution. The Y-architecture, in which pads are arranged in an equilateral lattice and the power

mesh is also arranged in an equilateral grid, is considered by Chen *et al.* [3]. Analytical and simulation results are obtained, which indicate a 5% reduction in the maximum voltage drop in the case of a single layer Y-architecture compared with the single layer Manhattan architecture.

Aquareles *et al.* [2] put the mathematical aspects of the work of Shakeri and Meindl [9] on a firm footing. They obtain an asymptotic formula for the maximum voltage drop in terms of the size of the pads, including higher order terms that would seem to be beyond the techniques in Shakeri and Meindl [9]. The main mathematical tool they use is that of matched asymptotic expansions. In the present work, we use a complex analysis method to derive an expression for the maximum voltage drop in the case of the square pad arrangement. This method is simpler and more direct than the approach in Aquareles *et al.* [2] and covers, without additional effort, the case of pads arranged in an equilateral triangular array. With a little extra work, the method extends to treat the case of pads arranged in a hexagonal pattern, thereby covering all three regular arrangements of power pads.

The results that we obtain suggest that the smaller maximum voltage drops observed by Chen *et al.* in [3] are due to the arrangement of pads in an equilateral array. Note that the various interconnection architectures considered in [3] could potentially be thought to contribute to a reduced voltage drop. In our model, the power pads are connected to a mesh of perpendicular wires that appear in the idealised mathematical model as a non-homogeneous term in the Poisson equation. Our results show that, irrespective of any other design variations, the arrangement of power pads alone can account for the smaller voltage drop reported in [3].

We also obtain formulas for the maximum voltage drop in each of these configurations (square, triangular, and hexagonal). It is found that the hexagonal pad arrangement has the largest voltage drop of the three configurations considered. Nonetheless, it may be useful to have an explicit formula for the voltage drop in this case since, however important, control of the maximum voltage drop is but one of several constraints in the design of an on-chip PDN. Finally, the availability of explicit formulas makes it possible to accurately predict the maximum voltage drop at an early point in the circuit design stage, thereby obviating the need for costly redesign.

2 Mathematical model of the voltage drop

In this section, we describe the mathematical model of the PDN and the associated voltage drop as derived by Shakeri and Meindl [9].

The surface of the integrated circuit is modelled as an infinite complex plane in which the power pads of the PDN are modelled as circular disks of radius ε . Power to the chip is supplied through these power pads and distributed through a fine grid of wires called the power mesh. The square and triangular arrangements of the pads are displayed below. The planar region consisting of the complex plane with these circular disks removed is denoted by Ω_ε . Under the assumption of uniform current flow between pads, the voltage drop satisfies the equation $\Delta u = c$ as the power mesh becomes finer.

The constant c on the right-hand side of this partial differential equation codes for the resistance properties of the wires of the mesh and the current drawn from the power

network. In order to make a fair comparison between the voltage drop across different PDN configurations, the resistance properties of the underlying integrated circuits (IC) and the current drawn need to be the same, that is, we need to use the same constant c in all cases. Moreover, since we measure the relative change in the maximum voltage drop across different arrangements of power pads, and since the solution to $\Delta u = c$ is proportional to c , it suffices to take the common value $c = 1$ in the modelling equation. Next, the power distribution pads are held at a constant voltage, which we may take to equal zero. Thus, the governing partial differential equation for the voltage in the region Ω_ε between the power pads is

$$\begin{cases} \Delta u = 1 & \text{in } \Omega_\varepsilon, \\ u = 0 & \text{on } \partial\Omega_\varepsilon. \end{cases} \quad (2.1)$$

The voltage between the pads will then be negative, since u is subharmonic and the pads themselves are held at voltage 0, while the voltage drop relative to the pads will simply be $-u$. It is interesting to note that the solution of the partial differential equation $\Delta u = -2$ in a domain D , also with zero Dirichlet boundary conditions, describes the expected exit time of standard Brownian motion from the domain. Thus, the problem of determining the maximum voltage drop is mathematically equivalent to determining the maximum expected lifetime of Brownian motion in the domain complementary to the power pads.

The partial differential equation (2.1) obeys the scaling law: If $u(z)$ is a solution of $\Delta_z u = 1$ in the domain D , then $v(w) = r^2 u(w/r)$ is a solution of $\Delta_w v = 1$ in the domain rD . Thus, if both the radius of the power pads and the spacing between their centres change by a factor of r , then the maximum voltage drop changes by a factor r^2 . If we know the voltage drop for all values of the radius of power pads for some *fixed* spacing between their centres, then we can scale this result to determine the voltage drop in the case of any power pad radius and any spacing between their centres.

Next, in order to make a fair comparison between different geometric power pad configurations, the proportion of the area on the chip occupied by the power pads (let's call it p) should be the same in each case. Note that p , the area of the power pads per unit area on the chip, does not change under the scaling $z \rightarrow rz$ discussed above, whereas the voltage drop changes by a factor r^2 . Thus, even for prescribed areal density p of power pads, the voltage drop can be made as small as one wishes by taking smaller pads closer together. In order to make a fair comparison between different configurations, it is therefore not only necessary to ensure that the areal density of the power pads is the same in each configuration but also to specify the radius ε of each pad. The values of p and ε then determine the spacing between the pads. (Alternatively, one could instead specify the spacing between the pads rather than their radius, but this seems less natural.)

Referring to Figure 1, each pad in the square arrangement lies at centre of a square of side d_1 , which does not overlap with the corresponding square for any other pad. Thus, the areal density p is $\pi\varepsilon^2/d_1^2$ in this case. For an equilateral triangular arrangement, each pad lies at the centre of a diamond of area $\sqrt{3}d_2^2/2$, which does not overlap with the corresponding diamond for any other pad. Thus, the areal density p of the pads in the triangular configuration is $2\pi\varepsilon^2/(\sqrt{3}d_2^2)$. For prescribed common radius ε of the pads, the

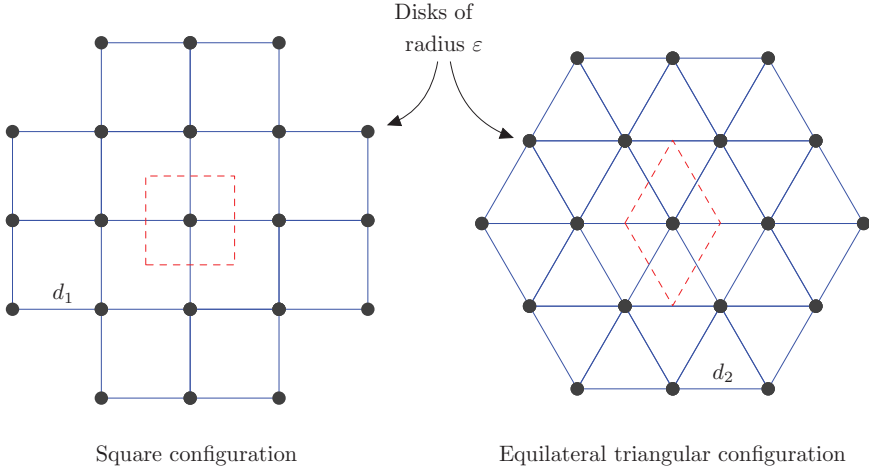


FIGURE 1. (Colour online) Square and equilateral triangular arrangements of pads.

areal density of the pads will be the same in both configurations once

$$d_2^2 = \frac{2}{\sqrt{3}} d_1^2. \quad (2.2)$$

Assuming, therefore, that in the square arrangement we have power pads of radius ε whose centres are unit distance apart, in the triangular arrangement we should have power pads of radius ε whose centres are $d_2 = \sqrt{2}/\sqrt[4]{3} \simeq 1.0745$ apart.

In the case of the hexagonal configuration, as shown in Figure 2, each pad lies at the centre of an equilateral triangle of sidelength $\sqrt{3} d_3$ which does not overlap with the corresponding triangle for any other pad. The area of this triangle is $\sqrt{3}(\sqrt{3} d_3)^2/4 = 3\sqrt{3} d_3^2/4$ so that the areal density p for the hexagonal configuration is $4\pi\varepsilon^2/(3\sqrt{3} d_3^2)$. In order that this agrees with the areal density $p = \pi\varepsilon^2$ for the previous configurations, we need

$$d_3 = \frac{2}{\sqrt[4]{27}} \simeq 0.87738.$$

In this case, each hexagon has area 2.

3 Main numerical results

Analytic formulas for voltage drop in each of the arrangements of the pads considered above are established in Sections 4 and 5. These yield the following bounds for the maximum voltage drop. In terms of the radius ε of pads, the maximum voltage drop V_{\max}^S in the case of the square arrangement is

$$V_{\max}^S(\varepsilon) = \frac{1}{2\pi} \log \frac{1}{\varepsilon} - 0.153418893205 + \frac{1}{4}\varepsilon^2 + O(\varepsilon^3). \quad (3.1)$$

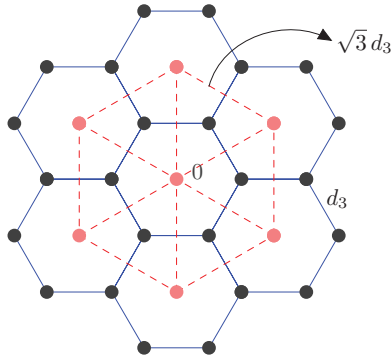


FIGURE 2. (Colour online) Regular hexagonal configuration.

The maximum voltage drop V_{\max}^T in the case of the triangular configuration is

$$V_{\max}^T(\varepsilon) = \frac{1}{2\pi} \log \frac{1}{\varepsilon} - 0.166549975068 + \frac{1}{4}\varepsilon^2 + O(\varepsilon^6). \quad (3.2)$$

In the case of the hexagonal configuration, the voltage drop at the centre of a hexagon is

$$V^H(\varepsilon) = \frac{1}{2\pi} \log \frac{1}{\varepsilon} - 0.111391075030 + \frac{1}{4}\varepsilon^2 + O(\varepsilon^3). \quad (3.3)$$

It is notable that, apart from the error term, the maximum voltage drop has the same dependence on pad size in all three cases, the only difference being in the constant term. The conclusion is that the hexagonal pad arrangement has the worst (that is, the largest) voltage drop among the configurations that we consider, the best being the triangular lattice, with the standard square lattice being in an intermediate position.

One intuitive explanation of this situation is that though in the hexagonal arrangement, there are six disks around the origin, these are, crucially, further separated from the origin than in the other configurations considered. It is possible to fit a bigger disk around the origin which does not meet the boundary of Ω_ε and this allows the Brownian motion to increase its expected lifespan.

Theorem 2 provides explicit upper and lower bounds on the maximum voltage drop in each configuration, with explicit constants. These bounds imply (3.1), (3.2) and (3.3) and are plotted in Figure 3. The curves represent upper and lower bounds for the maximum voltage drops $V_{\max}^S(\varepsilon)$ and $V_{\max}^T(\varepsilon)$, which take account of explicit error terms in Theorem 2. The plot in the hexagonal case shows the voltage drop $V^H(\varepsilon)$ at the centre of a hexagon. Presumably, this is the maximum voltage drop, that is, the maximum voltage drop presumably occurs at the centre of a hexagon, but in any case the maximum voltage drop is at least this large. Thus, even at the limits of the error bounds, the triangular arrangement outperforms the square and hexagonal arrangements for all pad sizes. Note also that the error bounds are seen to be quite tight in both square and triangular configurations so that formulas (3.1) and (3.2) are accurate. Note that the range of pad size ε (from 0.1 to 0.3) relative to the distance between the centres of the pads (d_1 , d_2 , d_3 , each of which is about unit size) is informed by industry norms (see [9, Table III]).

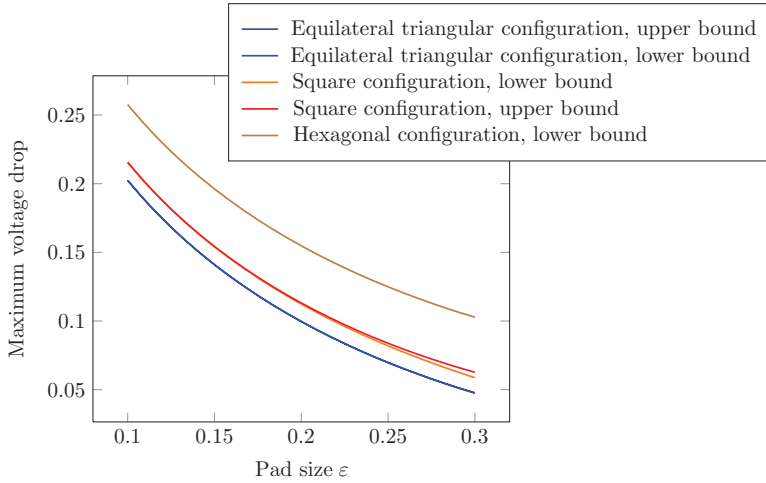


FIGURE 3. (Colour online) Plots of explicit bounds for maximum voltage drop as a function of pad size – see Theorem 2 [(4.31) and (4.33)] and Section 5. (Note that the upper and lower bounds in the equilateral triangular configuration are so close as to be effectively indistinguishable.)

Table 1. *Voltage drop measurements*

	Square arrangement	Triangular arrangement
On board measurement	2.03 V	1.91 V
SPICE simulation	2.05 V	1.94 V

In order to test the robustness of these analytical results we assembled two boards, each with a rectangular mesh of resistances. A constant current sink was connected at each node. On one of the boards, the voltage distribution was through a collection of pads in a square configuration, and on the other the pads were in a triangular configuration. All pads were held at 5 V. The maximum voltage drop was measured for each board. It was 1.91 V in the triangular pad setting versus 2.03 V in the square setting. The Simulation Program with Integrated Circuit Emphasis (SPICE) simulations with the same configuration returned voltage drops of 1.94 V in the triangular case and 2.05 V in the square case (see Table 1). The difference between the on-board measurements and the SPICE simulations may be due to less than perfect current sinks.

4 Analytic expression for the voltage drop in square and triangular pad arrays

In this section, analytic expressions for the voltage drop in both square and triangular pad arrangements are obtained. Both configurations correspond to lattices in the plane, permitting direct use of the standard theory of elliptic functions. We next set out those aspects of the theory that we will need, as well as the special results that pertain for square and equilateral lattices, drawing on the classic text by Hille [6, Section 13.2] as a standard general reference.

4.1 Square and triangular lattices

A lattice of points in the complex plane consists of all integer linear combinations $2w_1m + 2w_3n$ ($m, n \in \mathbb{Z}$) of two given complex numbers $2w_1$ and $2w_3$ for which w_3/w_1 has positive imaginary part. We immediately specialize to the case in which

$$2w_1 = d > 0 \quad \text{and} \quad 2w_3 = \alpha d, \quad \text{where } \alpha = e^{2\pi i/q}, \quad q \in \mathbb{N}, \quad (4.1)$$

so that α is a q th root of unity. In this case the lattice is described by

$$A = \{\lambda_{m,n} = md + n\alpha d : m, n \in \mathbb{Z}\}. \quad (4.2)$$

The resulting lattice is invariant under multiplication by α precisely when there are integers k and j such that

$$e^{4\pi i/q} = \alpha^2 = k\alpha + j = ke^{2\pi i/q} + j.$$

It is not difficult to see, for example by examining the resulting equations for the real and imaginary parts separately, that α will satisfy such an identity only in the cases $q = 4$ and $q = 6$. The case $q = 4$, with $\alpha = i$, $2w_3 = id$, $\alpha^2 = -1$, corresponds to the square lattice. The case $q = 6$, with $\alpha = e^{\pi i/3}$, $2w_3 = e^{\pi i/3}d$, $\alpha^2 = \alpha - 1$, corresponds to the triangular lattice. The values of d in each case are governed by (2.2), which guarantee that the areal densities of the pads agree.

Much of the analysis in the next sections is essentially unchanged whether we work with the square or triangular lattice. We will therefore retain the notation q , d , α with the understanding that

$$(q, d, \alpha) = \begin{cases} (4, 1, i) & \text{in the square lattice case,} \\ \left(6, \frac{\sqrt{2}}{\sqrt{3}}, e^{\pi i/3}\right) & \text{in the triangular lattice case,} \end{cases} \quad (4.3)$$

the advantage being that in this way we can treat both configurations simultaneously.

4.2 The Weierstrass σ -function for a plane lattice

The Weierstrass σ -function associated with the previously defined lattice is given by

$$\sigma(z) = z \prod'_{\lambda \in A} \left(1 - \frac{z}{\lambda}\right) \exp\left(\frac{z}{\lambda} + \frac{z^2}{2\lambda^2}\right), \quad (4.4)$$

where \prod' denotes the product over all lattice points with zero omitted. The Weierstrass ζ -function is defined by

$$\zeta(z) = \frac{1}{z} + \sum'_{\lambda \in A} \left(\frac{1}{z - \lambda} + \frac{1}{\lambda} + \frac{z}{\lambda^2}\right), \quad (4.5)$$

where \sum' denotes the sum over all lattice points with zero omitted.

A quasi-periodicity property of the σ -function plays a key role in our analysis. Set

$$\eta_1 = \zeta(w_1) \quad \text{and} \quad \eta_3 = \zeta(w_3).$$

Then [6, Identity 13.2.19],

$$\sigma(z + 2w_k) = -e^{2\eta_k(z+w_k)} \sigma(z), \quad z \in \mathbf{C}, \quad k = 1, 3. \quad (4.6)$$

Identity (4.6) with $k = 1$ and 3 , together with Legendre's identity (see [6, Exercise 13.2.4])

$$2w_3\eta_1 - 2w_1\eta_3 = i\pi, \quad (4.7)$$

leads to the full quasi-periodicity property

$$\sigma(z + 2mw_1 + 2nw_3) = (-1)^{m+n+mn} \exp[(z + mw_1 + nw_3)(2m\eta_1 + 2n\eta_3)] \sigma(z) \quad (4.8)$$

for any integers m and n . To proceed further, we need to compute η_1 and η_3 explicitly for square and triangular lattices, at which point the quasi-periodicity property (4.8) will become explicit in these cases. While these results are known, here we give explicit computations for completeness.

4.3 Computation of η_1 and η_3 for square and triangular lattices

Identity (4.7) in the case of either of our lattices becomes (see (4.1))

$$d\alpha\eta_1 - d\eta_3 = i\pi. \quad (4.9)$$

The invariance of the lattice under multiplication by $\alpha = e^{2\pi i/q}$ and its powers, with $q = 4$ for the square lattice and $q = 6$ for the triangular lattice, leads to a second linear relationship between η_1 and η_3 as follows. By definition,

$$\eta_1 = \zeta\left(\frac{d}{2}\right) = \frac{2}{d} + \sum'_{\lambda \in \mathcal{A}} \left(\frac{1}{d/2 - \lambda} + \frac{1}{\lambda} + \frac{d}{2\lambda^2} \right).$$

Replacing λ by $\alpha^k \lambda$, $k = 1, \dots, q-1$, gives a total of q expressions for η_1 . Adding these leads to

$$\eta_1 = \frac{2}{d} + \frac{1}{q} \sum'_{\lambda \in \mathcal{A}} \sum_{k=0}^{q-1} \left(\frac{1}{d/2 - \alpha^k \lambda} + \frac{1}{\alpha^k \lambda} + \frac{d}{2\alpha^{2k} \lambda^2} \right).$$

Since

$$\sum_{k=0}^{q-1} \alpha^{-k} = 0 = \sum_{k=0}^{q-1} \alpha^{-2k}, \quad (4.10)$$

we find that

$$\eta_1 = \frac{2}{d} + S, \quad \text{where } S = \frac{1}{q} \sum'_{\lambda \in \mathcal{A}} \sum_{k=0}^{q-1} \frac{1}{d/2 - \alpha^k \lambda}. \quad (4.11)$$

This procedure is repeated for η_3 , which is given by

$$\eta_3 = \zeta\left(\frac{d\alpha}{2}\right) = \frac{2}{d\alpha} + \sum'_{\lambda \in \mathcal{A}} \left(\frac{1}{d\alpha/2 - \lambda} + \frac{1}{\lambda} + \frac{d\alpha}{2\lambda^2} \right).$$

Replacing λ by $\alpha^k \lambda$, $k = 1, \dots, q-1$, and adding all q expressions for η_3 , leads to

$$\begin{aligned}
 \eta_3 &= \frac{2}{d\alpha} + \frac{1}{q} \sum'_{\lambda \in \mathcal{A}} \sum_{k=0}^{q-1} \left(\frac{1}{d\alpha/2 - \alpha^k \lambda} + \frac{1}{\alpha^k \lambda} + \frac{d\alpha}{2\alpha^{2k} \lambda^2} \right). \\
 &= \frac{2}{d\alpha} + \frac{1}{q} \sum'_{\lambda \in \mathcal{A}} \sum_{k=0}^{q-1} \frac{1}{d\alpha/2 - \alpha^k \lambda} \\
 &= \frac{2}{d\alpha} + \frac{1}{q\alpha} \sum'_{\lambda \in \mathcal{A}} \sum_{k=0}^{q-1} \frac{1}{d/2 - \alpha^k \lambda} \\
 &= \frac{2}{d\alpha} + \frac{1}{\alpha} S = \left(\frac{2}{d} + S \right) \frac{1}{\alpha}.
 \end{aligned} \tag{4.12}$$

Together, (4.11) and (4.12) yield

$$\eta_1 = \alpha \eta_3. \tag{4.13}$$

Solving the simultaneous equations (4.9) and (4.13) gives

$$\eta_1 = \frac{i\alpha\pi}{d(\alpha^2 - 1)} \quad \text{and} \quad \eta_3 = \frac{i\pi}{d(\alpha^2 - 1)}. \tag{4.14}$$

Lemma 1 *In the case of the square lattice ($d = 1$, $\alpha = i$)*

$$\eta_1 = \frac{\pi}{2} \quad \text{and} \quad \eta_3 = -\frac{i\pi}{2}, \tag{4.15}$$

while in the case of the triangular lattice ($d = \sqrt{2}/\sqrt[4]{3}$, $\alpha = e^{\pi i/3}$),

$$\eta_1 = \frac{\pi}{\sqrt{2}\sqrt[4]{3}} \quad \text{and} \quad \eta_3 = \frac{\pi}{\sqrt{2}\sqrt[4]{3}} e^{-\pi i/3}. \tag{4.16}$$

These results are easily verified, in view of (4.1), by replacing α by i and d by 1 in (4.14) in the case of the square lattice to obtain (4.15). In the case of the triangular lattice, replace α by $e^{\pi i/3}$ in (4.14) and use

$$\alpha^2 - 1 = -\frac{3}{2} + \frac{\sqrt{3}}{2}i = \sqrt{3}i \left(\frac{1}{2} + \frac{\sqrt{3}}{2}i \right) = \sqrt{3}i\alpha$$

to obtain $\eta_1 = \pi/(\sqrt{3}d)$ and $\eta_3 = \pi/(\sqrt{3}d\alpha) = \pi\bar{\alpha}/(\sqrt{3}d)$. Finally, set $d = \sqrt{2}/\sqrt[4]{3}$ to obtain (4.16).

4.4 Quasi-periodicity and true periodicity for square and triangular lattices

These values for η_1 and η_3 lead to a simple form of the general quasi-periodicity relation (4.8) for the σ -function in the case of square and triangular lattices. Surprisingly, perhaps, this relation has the same form in both cases, thereby unifying the analysis required to

derive an analytic expression for IR-drop. With an eye on (4.8), recall that a general lattice point is $\lambda_{m,n} = 2w_1m + 2w_3n = md + n\alpha d$, where m and n are integers. Then in the case of a square lattice with $d = 1$ and using the η -values given by (4.15),

$$\lambda_{m,n} = m + in \quad \text{and} \quad 2m\eta_1 + 2n\eta_3 = m\pi - in\pi = \pi \overline{\lambda_{m,n}}.$$

In the case of a triangular lattice with $d = \sqrt{2}/\sqrt[4]{3}$, we use the η -values given by (4.16) to obtain

$$\begin{aligned} \lambda_{m,n} &= \frac{\sqrt{2}}{\sqrt[4]{3}} m + \frac{\sqrt{2}}{\sqrt[4]{3}} e^{\pi i/3} n, \\ 2m\eta_1 + 2n\eta_3 &= \frac{2m\pi}{\sqrt{2}\sqrt[4]{3}} + \frac{2n\pi}{\sqrt{2}\sqrt[4]{3}} e^{-\pi i/3} = \pi \left(\frac{\sqrt{2}}{\sqrt[4]{3}} m + \frac{\sqrt{2}}{\sqrt[4]{3}} e^{-\pi i/3} n \right) = \pi \overline{\lambda_{m,n}}. \end{aligned}$$

The quasi-periodicity property (4.8) of the σ -function, in the case of either square or triangular lattice, therefore becomes

$$\begin{aligned} \sigma(z + \lambda_{m,n}) &= (-1)^{m+n+mn} \exp \left[\left(z + \frac{1}{2} \lambda_{m,n} \right) \pi \overline{\lambda_{m,n}} \right] \sigma(z) \\ &= (-1)^{m+n+mn} \exp \left[\pi \overline{\lambda_{m,n}} z + \frac{\pi}{2} |\lambda_{m,n}|^2 \right] \sigma(z). \end{aligned} \quad (4.17)$$

This quasi-periodicity property of the σ -function leads to true periodicity of a related function.

Lemma 2 *Set*

$$h(z) = -\frac{1}{2\pi} \log |\sigma(z)| + \frac{1}{4} |z|^2, \quad z \in \mathbf{C} \setminus A. \quad (4.18)$$

In the case when either A is a square lattice or a triangular lattice, h is periodic in the sense that $h(z + \lambda) = h(z)$, for $z \in \mathbf{C} \setminus A$, $\lambda \in A$.

Furthermore, the value of h doesn't change under reflection in any side of relevant lattice, in that

$$h(\alpha^{2k} \bar{z}) = h(z), \quad (4.19)$$

where $\alpha = i$ and $k = 0$ or 1 in the square lattice case, while $\alpha = e^{\pi i/3}$ and $k = 0, 1$ or 2 in the triangular lattice case.

Remark 1 *The periodicity of h in the case of square or triangular lattices also follows from the results in [4, Proposition 3.4] which builds upon work in [5]. Gröchenig and Lyubarskii [4] have a more general periodicity result which is valid for all lattices and involves an explicit normalization factor in terms of η_1 and η_3 . The computation of η_1 and η_3 above shows that no normalization factor arises for triangular or square lattices.*

Proof Taking the logarithm of (4.17) with $\lambda = \lambda_{m,n} \in A$ leads to

$$\log |\sigma(z + \lambda)| = \log |\sigma(z)| + \operatorname{Re} \left[\pi \bar{\lambda} z + \frac{\pi}{2} |\lambda|^2 \right] = \log |\sigma(z)| + \frac{\pi}{2} [|\lambda|^2 + 2 \operatorname{Re}(\bar{\lambda} z)].$$

But

$$|\lambda|^2 + 2 \operatorname{Re}(\bar{\lambda} z) = |z + \lambda|^2 - |z|^2,$$

so that

$$\log |\sigma(z + \lambda)| = \log |\sigma(z)| + \frac{\pi}{2} [|z + \lambda|^2 - |z|^2].$$

This establishes the periodicity of h .

To establish that h is invariant under reflection on any side of the lattice, note that in any of the cases in (4.19),

$$\sigma(\alpha^{2k} \bar{z}) = \alpha^{2k} \bar{z} \prod'_{\lambda \in \mathcal{A}} \left(1 - \frac{\alpha^{2k} \bar{z}}{\lambda} \right) \exp \left(\frac{\alpha^{2k} \bar{z}}{\lambda} + \frac{\alpha^{4k} \bar{z}^2}{2\lambda^2} \right).$$

The invariance of the lattice under multiplication by α^{2k} , that is, $\alpha^{2k} \mathcal{A} = \mathcal{A}$, and then its invariance under complex conjugation, shows that

$$\begin{aligned} \sigma(\alpha^{2k} \bar{z}) &= \alpha^{2k} \bar{z} \prod'_{\lambda \in \mathcal{A}} \left(1 - \frac{\bar{z}}{\lambda} \right) \exp \left(\frac{\bar{z}}{\lambda} + \frac{\bar{z}^2}{2\lambda^2} \right) \\ &= \alpha^{2k} \overline{\left(z \prod'_{\lambda \in \mathcal{A}} \left(1 - \frac{z}{\bar{\lambda}} \right) \exp \left(\frac{z}{\bar{\lambda}} + \frac{z^2}{2\bar{\lambda}^2} \right) \right)} \\ &= \alpha^{2k} \overline{\left(z \prod'_{\lambda \in \mathcal{A}} \left(1 - \frac{z}{\lambda} \right) \exp \left(\frac{z}{\lambda} + \frac{z^2}{2\lambda^2} \right) \right)} \\ &= \alpha^{2k} \overline{\sigma(z)}. \end{aligned} \tag{4.20}$$

On taking logarithms, the identity (4.19) follows. \square

4.5 Analytic expressions for IR-drop in square and triangular arrangements

Formally, $\Omega_\varepsilon = \mathbf{C} \setminus \bigcup_{\lambda \in \mathcal{A}} \bar{D}(\lambda, \varepsilon)$ denotes the region formed by removing from the plane a closed disk of radius ε about each lattice point. Our main result gives an analytic bound for the voltage drop in both square and triangular arrangements of pads. It is possible to analyse both configurations simultaneously, which we do. After stating and proving the analytic bound, we derive explicit numerical bounds (3.1) and (3.2), which prove, in particular, that the triangular disposition outperforms the square arrangement.

Before stating the main analytical result, Theorem 1, we need an estimate on the σ -function near the origin.

Lemma 3 For $|z|^q \leq \frac{3}{5}$,

$$|\log |\sigma(z)| - \log |z|| \leq A_q (|z|^q + |z|^{2q}), \tag{4.21}$$

where $A_q = \frac{1}{q} \sum'_{\lambda \in \mathcal{A}} \frac{1}{|\lambda|^q}$ and where q is 4 or 6 depending on whether we are working with

the square or the triangular lattice. Correct to eight decimal places,

$$A_4 = \frac{1}{4} \sum'_{\lambda \in \mathcal{A}} \frac{1}{(m^2 + n^2)^2} = 1.50670300 \quad (4.22)$$

and

$$A_6 = \frac{\sqrt{3}}{16} \sum'_{\lambda \in \mathcal{A}} \frac{1}{(m^2 + n^2 + mn)^3} = 0.69020942. \quad (4.23)$$

Proof Recall expression (4.4) for the σ -function. By the symmetry of the lattice under multiplication by α^k , we see that

$$\sigma(z) = z \prod'_{\lambda \in \mathcal{A}} \left(1 - \frac{z}{\alpha^k \lambda}\right) \exp\left(\frac{z}{\alpha^k \lambda} + \frac{z^2}{2\alpha^{2k} \lambda^2}\right), \quad k = 0, 1, \dots, q-1.$$

When these q expressions for $\sigma(z)$ are multiplied together, one obtains

$$\sigma^q(z) = z^q \prod'_{\lambda \in \mathcal{A}} \prod_{k=0}^{q-1} \left(1 - \frac{z}{\alpha^k \lambda}\right) = z^q \prod'_{\lambda \in \mathcal{A}} \left(1 - \frac{z^q}{\lambda^q}\right), \quad (4.24)$$

where (4.10) leads to the elimination of exponential terms and the identity

$$1 - w^q = (1 - w) \left(1 - \frac{w}{\alpha}\right) \dots \left(1 - \frac{w}{\alpha^{q-1}}\right), \quad q \in \mathbb{N},$$

was used at the last step in (4.24). Taking the logarithm of (4.24) leads to

$$\log |\sigma(z)| = \log |z| + \frac{1}{q} \sum'_{\lambda \in \mathcal{A}} \log \left|1 - \frac{z^q}{\lambda^q}\right|. \quad (4.25)$$

The power series expansion of the analytic function $-\log(1 - w)$ about 0 is

$$-\log(1 - w) = w + \frac{w^2}{2} + \frac{w^3}{3} + \frac{w^4}{4} + \dots,$$

so that, for $|w| \leq \frac{3}{5}$,

$$\begin{aligned} |\log |1 - w|| &= |\operatorname{Re}(\log(1 - w))| \\ &\leq |\log(1 - w)| \\ &\leq |w| + \frac{|w|^2}{2} + \frac{|w|^3}{3} + \frac{|w|^4}{4} + \dots \\ &\leq |w| \left(1 + \frac{|w|}{2} + \frac{|w|^2}{3} \frac{1}{1 - |w|}\right) \leq (1 + |w|) |w|. \end{aligned} \quad (4.26)$$

Since $|\lambda| \geq 1$ for $\lambda \in \mathcal{A} \setminus \{0\}$, once $|z|^q \leq \frac{3}{5}$ we can apply (4.26) with $w = (z/\lambda)^q$ to obtain

$$\left| \frac{1}{q} \sum'_{\lambda \in \mathcal{A}} \log \left|1 - \frac{z^q}{\lambda^q}\right| \right| \leq \frac{1}{q} \sum'_{\lambda \in \mathcal{A}} \left(\frac{|z|^q}{|\lambda|^q} + \frac{|z|^{2q}}{|\lambda|^{2q}} \right) \leq A_q (|z|^q + |z|^{2q}),$$

where

$$A_q = \frac{1}{q} \sum'_{\lambda \in \mathcal{A}} \frac{1}{|\lambda|^q}.$$

Together with (4.25), this proves (4.21). Estimates (4.22) and (4.23) can be obtained numerically. \square

Theorem 1 *In the case of either the square or the triangular lattice, in each case with the values given in (4.3), the solution of*

$$\begin{cases} \Delta u_\varepsilon = 1 & \text{in } \Omega_\varepsilon \\ u_\varepsilon = 0 & \text{on } \partial\Omega_\varepsilon \end{cases} \quad (4.27)$$

may be written as

$$u_\varepsilon(z) = -\frac{1}{2\pi} \log |\sigma(z)| + \frac{1}{4} |z|^2 + \frac{1}{2\pi} \log \varepsilon - \frac{1}{4} \varepsilon^2 + h_\varepsilon(z), \quad (4.28)$$

where h_ε satisfies

$$|h_\varepsilon(z)| \leq \frac{A_q}{2\pi} (\varepsilon^q + \varepsilon^{2q}), \quad z \in \Omega_\varepsilon, \quad (4.29)$$

and A_q has the value given in the statement of Lemma 3.

Proof Let h_ε be the function which is harmonic on Ω_ε and has boundary values

$$h_\varepsilon(w) = \frac{1}{2\pi} \log |\sigma(w)| - \frac{1}{4} |w|^2 - \frac{1}{2\pi} \log \varepsilon + \frac{1}{4} \varepsilon^2, \quad w \in \partial\Omega_\varepsilon. \quad (4.30)$$

By Lemma 2, these boundary values are periodic and so too is h_ε (that is, $h_\varepsilon(z + \lambda) = h_\varepsilon(z)$ for $z \in \Omega_\varepsilon$ and $\lambda \in \mathcal{A}$).

Define a function u_ε by (4.28). Then $\Delta u_\varepsilon = 1$ in Ω_ε . This is because $\Delta(|z|^2) = 4$, while $\log |\sigma(z)|$ is harmonic on Ω_ε being the logarithm of the modulus of a non-vanishing analytic function there. Moreover, u_ε vanishes on the boundary of Ω_ε , so that u_ε is the solution of (4.27).

Set D_0 to be the interior of the square with vertices $0, 1, 1+i$ and i in the square lattice case, and set D_0 to be the interior of the triangle with vertices $0, \sqrt{2}/\sqrt[4]{3}$ and $\sqrt{2}e^{\pi i/3}/\sqrt[4]{3}$ in the triangular lattice case. Bound (4.29) for h_ε is obtained by applying the maximum principle to h_ε on $\Omega_\varepsilon \cap D_0$. If h_ε were to assume an extremal value on the closure of $\Omega_\varepsilon \cap D_0$ at a point of $\Omega_\varepsilon \cap \partial D_0$, then by the symmetry of h_ε in the sides of D_0 (see the final part of Lemma 2), h_ε would have a local extremum there, contradicting the maximum principle. Thus, h_ε achieves its extremum values (over Ω_ε or, equivalently, over $\Omega_\varepsilon \cap D_0$) at a point of $\partial\Omega_\varepsilon$, that is, again using the periodicity of h_ε , at a point on the circle $C(0, \varepsilon)$. Taking account of the boundary values (4.30) and then Lemma 3, we see that, for $|w| = \varepsilon$,

$$|h_\varepsilon(w)| = \frac{1}{2\pi} |\log |\sigma(w)| - \log \varepsilon| \leq \frac{A_q}{2\pi} (\varepsilon^p + \varepsilon^{2p}).$$

Thus, by the maximum principle, the harmonic function h_ε satisfies the bound (4.29) throughout Ω_ε . \square

Theorem 2 *The maximum voltage drop $V_{\max}^S(\varepsilon)$, when the pads are arranged in a square lattice and with the parameters given in (4.3), satisfies*

$$\left| V_{\max}^M(\varepsilon) - \left[\frac{1}{2\pi} \log \frac{1}{\varepsilon} - C_M + \frac{1}{4} \varepsilon^2 \right] \right| \leq \frac{A_4}{2\pi} (\varepsilon^4 + \varepsilon^8), \quad (4.31)$$

where A_4 is given by (4.22) and

$$C_M = \frac{1}{\pi} \log \Gamma\left(\frac{1}{4}\right) - \frac{1}{2\pi} \log(2\sqrt{2\pi}) = 0.153418893205, \quad (4.32)$$

correct to 12 decimal places.

The maximum voltage drop $V_{\max}^T(\varepsilon)$, when the pads are arranged in a triangular lattice and with the parameters given in (4.3), satisfies

$$\left| V_{\max}^T(\varepsilon) - \left[\frac{1}{2\pi} \log \frac{1}{\varepsilon} - C_Y + \frac{1}{4} \varepsilon^2 \right] \right| \leq \frac{A_6}{2\pi} (\varepsilon^6 + \varepsilon^{12}), \quad (4.33)$$

where A_6 is given by (4.23) and

$$C_Y = \frac{3}{2\pi} \log \Gamma\left(\frac{1}{3}\right) - \frac{1}{2\pi} \log(2\sqrt{2\pi}) + \frac{1}{8\pi} \log 3 = 0.166549975068, \quad (4.34)$$

correct to 12 decimal places.

Proof In the case of the square pad arrangement, the maximum voltage drop occurs at the point $b_s = (1 + i)/2$, which lies at the centre of the square formed by lattice points at 0, 1, $1 + i$ and i (see Section 6). Thus, the negative of expression (4.28), evaluated at $z = b_s$, is the maximum voltage drop. Since $|b_s|^2 = 1/2$,

$$V_{\max}^S = -u_\varepsilon(b_s) = \frac{1}{2\pi} \log \frac{1}{\varepsilon} - C_M + \frac{1}{4} \varepsilon^2 - h_\varepsilon(b_s),$$

where

$$C_M = \frac{1}{8} - \frac{1}{2\pi} \log |\sigma(b_s)|. \quad (4.35)$$

Formulas 18.14.7 and 18.14.9 in Abramowitz and Stegun [1] give

$$\sigma(w_2) = \sqrt{2} e^{(1+i)\pi/4} \quad \text{when} \quad w_1 = \frac{\Gamma^2(\frac{1}{4})}{4\sqrt{\pi}}, \quad w_3 = iw_1, \quad w_2 = w_1 + w_3.$$

Scaling by $t = 2\sqrt{\pi}/\Gamma^2(\frac{1}{4})$ so that $w_1 = 1/2$, and noting that the σ -function also scales linearly, we find that

$$\sigma(b_s) = \frac{2\sqrt{\pi}}{\Gamma^2(\frac{1}{4})} \sqrt{2} e^{(1+i)\pi/4}.$$

Then

$$\log |\sigma(b_s)| = \frac{\pi}{4} + \log(2\sqrt{2\pi}) - 2 \log \Gamma\left(\frac{1}{4}\right),$$

so that (4.32) follows from (4.35), and then (4.31) follows from the bound (4.29) for h_s .

In the case of the triangular pad arrangement, the maximum voltage drop occurs at the point

$$b_t = \frac{1}{\sqrt{3}} e^{\pi i/6} d = 3^{-3/4} \sqrt{2} e^{\pi i/6}$$

that lies at the centre of the equilateral triangle with vertices $0, 2w_1 = d, 2w_3 = d\alpha$, where $d = \sqrt{2}/\sqrt[4]{3}$ and $\alpha = e^{\pi i/3}$. Since $|b_t|^2 = 2/(3\sqrt{3})$,

$$V_{\max}^T(\varepsilon) = -u_\varepsilon(b_t) = \frac{1}{2\pi} \log \frac{1}{\varepsilon} - C_Y + \frac{1}{4} \varepsilon^2 - h_\varepsilon(b_t),$$

where

$$C_Y = \frac{1}{6\sqrt{3}} - \frac{1}{2\pi} \log |\sigma(b_t)|. \quad (4.36)$$

Formulas 18.13.15 and 18.13.28 in Abramowitz and Stegun [1] give the value of σ at the centre of the equilateral triangle [$\sigma(z_0)$ in their notation] as

$$\sigma\left(\frac{1}{\sqrt{3}} e^{\pi i/6} \tilde{d}\right) = e^{\pi/(3\sqrt{3})} e^{i\pi/6} \quad \text{when} \quad \tilde{d} = \frac{\Gamma^3(\frac{1}{3})}{2\pi}.$$

Scaling by $t = d/\tilde{d} = 2\pi\sqrt{2}/(\sqrt[4]{3}\Gamma^3(\frac{1}{3}))$ leads to the value

$$\sigma(b_t) = \frac{2\sqrt{2}\pi}{\sqrt[4]{3}\Gamma^3(\frac{1}{3})} e^{\pi/(3\sqrt{3})} e^{i\pi/6}$$

for the σ – function at the centre of a triangle in our lattice. Then,

$$\log |\sigma(b_t)| = \frac{\pi}{3\sqrt{3}} + \log(2\sqrt{2}\pi) - \frac{1}{4} \log 3 - 3 \log \Gamma(\frac{1}{3}),$$

(4.34) follows from (4.36), and then (4.33) again follows from the bound (4.29) for h_s . \square

5 The Hexagonal configuration

We estimate the voltage drop for a hexagonal lattice with the same areal density of pads as in the case of square and triangular power pad arrangements analysed in the previous section. The geometric setting is the following. We consider the domain

$$\Omega = \Omega_\varepsilon = \mathbf{C} \setminus \bigcup_{\lambda \in A} \overline{D}(\lambda, \varepsilon),$$

where A is the set of vertices of the blue hexagonal grid shown in Figure 2.

It will be convenient to view the set of centres A as the difference of two lattices: see Figure 2. The first lattice consists of black and red vertices in Figure 2, which we denote by BR , while the second lattice consists of red vertices alone, which we denote by R . Thus, $A = BR \setminus R$. Both BR and R are lattices that determine an equilateral grid. The main advantage of considering A as a difference between two lattices is that for any equilateral lattice we can construct an associated Weierstrass entire function with zeros on the lattice whose pseudo-periodicity properties were analysed in the previous section. Thus, instead

of directly building an entire function with zeros on A , we obtain more information by considering a quotient of two entire functions, one vanishing on BR and the other on R .

The maximum voltage drop corresponds to the minimum value of u , where u is the solution to $\Delta u = 1$ in Ω_ε and $u = 0$ in the boundary of Ω_ε . The maximum voltage drop is, consequently, at least as big as $-u(0)$, where 0 is at the centre of a hexagon.

Let us denote by $\sigma(z)$ the Weierstrass σ -function associated with the equilateral triangular lattice with side length $d_2 = \sqrt{2}/\sqrt[4]{3}$ as described in (4.3). The σ -function for the lattice BR , with sidelength $d_3 = 2/\sqrt[4]{27}$, is then

$$\sigma_{BR}(z) = \frac{d_3}{d_2} \sigma\left(\frac{d_2}{d_3} z\right) = \sqrt{\frac{2}{3}} \sigma\left(\sqrt{\frac{3}{2}} z\right),$$

while the σ -function for the lattice R , with sidelength $\sqrt{3}d_3$, is

$$\sigma_R(z) = \sqrt{2} \beta \sigma\left(\frac{1}{\sqrt{2} \beta} z\right), \text{ where } \beta = e^{\pi i/6}.$$

Clearly, σ_R vanishes on the vertices of R , and σ_{BR} vanishes on the vertices of BR .

Consider the function defined in Ω by

$$v(z) = v_{BR}(z) - v_R(z) = \left[\frac{3}{8} |z|^2 - \frac{1}{2\pi} \log |\sigma_{BR}(z)| - c_\varepsilon \right] - \left[\frac{1}{8} |z|^2 - \frac{1}{2\pi} \log |\sigma_R(z)| - d_\varepsilon \right],$$

where c_ε and d_ε are to be chosen appropriately. Both functions v_{BR} and v_R have many symmetries. In particular, they are symmetric across any line that extends any of the sides of the hexagon which form the original grid. Thus, v has the same symmetry. Moreover, $\Delta v = 1$ in Ω so that v is close to the desired solution u of the problem. In fact, they differ by a harmonic function in that $u = v + h$. The desired value $u(0)$ can be approximated by the value of v at the centre of the hexagon. The error that we make, that is $h(0)$, can again be estimated by the maximum principle, in that $|h(0)| \leq \sup_{\partial\Omega} |h| = \sup_{\partial\Omega} |v|$.

Constants c_ε and d_ε will now be chosen so that both $\sup_{\partial\Omega} v_{BR}$ and $\sup_{\partial\Omega} v_R$ are small. The selection of c_ε required to make v_{BR} small on the boundary is more straightforward. By the symmetries of v_{BR} , we have $\sup_{\partial\Omega} v_{BR} = \sup_{\partial D(0,\varepsilon)} v_{BR}$. Observe that although $\partial D(0,\varepsilon)$ is not part of the boundary of Ω , all disks around the vertices of the combined black and red triangular grid are equal if we restrict our attention to v_{BR} . On $\partial D(0,\varepsilon)$, the value of v_{BR} is close to a constant. In fact, we see from Lemma 3 that

$$v_{BR}(z) = \frac{3}{8} \varepsilon^2 + \frac{1}{2\pi} \log \frac{1}{\varepsilon} + O(\varepsilon^6) - c_\varepsilon, \quad \text{for all } z \in D(0,\varepsilon).$$

Thus, with the choice of $c_\varepsilon = \frac{1}{2\pi} \log \frac{1}{\varepsilon} + \frac{3}{8} \varepsilon^2$, we obtain that $|v_{BR}(z)| \leq C\varepsilon^6$ on $\partial\Omega_\varepsilon$.

We now consider the values of v_R on the boundary of Ω_ε which consists of disks of radius ε at the centres of red triangles. The function v_R has the same behaviour at each. Let us denote one of the centres by A . Then, as established in Section 6, v_R has a local minimum at A . We can actually prove that

$$v_R(z) = v_R(A) + \frac{1}{8} |z - A|^2 + O(\varepsilon^3), \quad \text{for all } z \in D(A,\varepsilon).$$

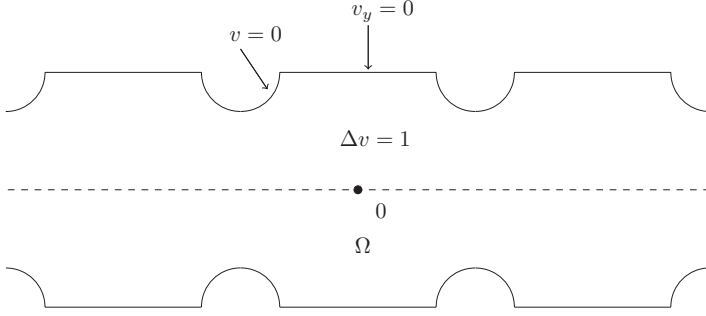


FIGURE 4. Auxiliary domain for square lattice.

Thus, if we choose $d_\varepsilon = \frac{1}{8}|A|^2 - \frac{1}{2\pi} \log |\sigma_R(A)| + \frac{1}{8}\varepsilon^2$, then $|v_R(z)| \leq C\varepsilon^3$ on $\partial D(A, \varepsilon)$ and therefore on $\partial\Omega_\varepsilon$.

Finally, we have proved that $\sup_{\partial\Omega_\varepsilon} |h| = \sup_{\partial\Omega_\varepsilon} |v| \leq C\varepsilon^3$. The voltage drop at the centre of a hexagon is $-u(0) = -v(0) - h(0)$, and so

$$V^H(\varepsilon) := -u(0) = c_\varepsilon - d_\varepsilon + O(\varepsilon^3) = \frac{1}{2\pi} \log \frac{1}{\varepsilon} - \frac{1}{8}|A|^2 + \frac{1}{2\pi} \log |\sigma_R(A)| + \frac{1}{4}\varepsilon^2 + O(\varepsilon^3).$$

Observe that $\log |\sigma_R(A)| = \log \sqrt{2} + \log |\sigma(A/(\beta\sqrt{2}))|$. In our setting $|A|^2 = 4/(3\sqrt{3})$ and the value of the σ -function at the centre of its defining triangle can be computed explicitly (see [1, Formula 18.13.28]), as

$$\left| \sigma\left(\frac{A}{\beta\sqrt{2}}\right) \right| = e^{\pi/(3\sqrt{3})} \frac{2\sqrt{2}\pi}{3^{1/4}\Gamma(1/3)^3} \simeq 0.642836690101.$$

Thus, the voltage drop at the centre of a hexagon is

$$V^H(\varepsilon) = \frac{1}{2\pi} \log \frac{1}{\varepsilon} - 0.111391075030 + \frac{1}{4}\varepsilon^2 + O(\varepsilon^3),$$

which is (3.3). The conclusion is that the hexagonal grid has the worst voltage drop among the ones that we considered, with the best being the triangular lattice, and the standard square lattice being in an intermediate position.

6 Where does the maximum voltage drop occur?

We now examine where the maximal voltage drop takes place in the square lattice configuration and in the triangular setting. Heuristically, one expects the voltage drop to be maximal at the centres of the squares and centres of the equilateral triangles respectively. This has been taken for granted in the literature, but we will nevertheless give a rigorous proof of this intuitive fact. The case of the square is the easier one.

Proof Consider the solution v in the unbounded domain Ω to the mixed Dirichlet–Neumann problem as in the Figure 4: We want to prove that it has a minimum value at $z = 0$. We will prove that the function $v_y > 0$ when $\Im z > 0$ and $v_y < 0$ when $\Im z < 0$.

Clearly,

$$\Delta v_y = \frac{\partial \Delta v}{\partial y} = \frac{\partial 1}{\partial y} = 0.$$

Thus, v_y is harmonic. Moreover, on the ‘straight’ pieces of the boundary, $v_y = 0$. The function v vanishes on the half circles, thus ∇v is perpendicular to these circles. Therefore, $v_y = \langle \nabla v, (0, 1) \rangle$ is positive on the half circles to the top of the dotted line and negative on all others. By symmetry, $v_y = 0$ on the dotted line. Thus, solving the Dirichlet problem for v_y in the domain $\Omega_+ := \Omega \cap \{\Im z > 0\}$, we see that $v_y \geq 0$ in Ω_+ (on the boundary it is positive) and $v_y \leq 0$ in $\Omega_- := \Omega \cap \{\Im z < 0\}$.

We argue similarly in the x -direction and we are done. \square

In the case of triangular lattice we consider the domain in Figure 5. The domain Ω is the equilateral triangle where we remove the three disks of equal radius centred at the corners of the triangle. Let p be the centre of the triangle and define the function u such that $\Delta u = 1$ in the interior of Ω , $u = 0$ on the part of the boundary of Ω defined by the arcs of circles and $\partial u / \partial n = 0$ on the part of the boundary of Ω defined by the sides of the triangle. The claim is the following:

Claim *There is only one minimum value of u in Ω and it is attained at p .*

Proof We will base this argument on a variation of the radius of disks. It will be convenient to denote by Ω_t the domain obtained by removing the disks of radius t and by u^t the corresponding solution. We will denote by v the Green’s function of the flat torus whose fundamental domain is twice the equilateral triangle. It follows from the definition that the Green’s function of this torus is the function $v(z) = \frac{1}{4}|z|^2 - \frac{1}{2\pi} \log |\sigma(z)|$, as we saw in Lemma 2. In a sense we will see that u^t is very close to v as $t \rightarrow 0$. We are interested in the critical points of u^t . The corresponding critical points for v have been identified in [7] and the only ones appearing are the trivial ones that can be identified by symmetry considerations. There is a local minimum of v at p and three saddle points at the midpoints of the sides of the triangle.

We are going to prove that a very similar structure arises in the case of u^t , namely that there is a minimum at p and three saddle points at the midpoints of the sides of the triangle.

Throughout this discussion we will restrict ourselves to the case $0 < t < t_0$, where t_0 is the largest radius such that the disks defining Ω_t are disjoint, since this is the only relevant case.

We begin by observing that u^t has a critical point at the centre p for symmetry reasons. Moreover, since $u^t(e^{2\pi i/3}(z-p)) = u^t(z-p)$, the Hessian of u^t at p must be a constant times the identity matrix. Since $\Delta u^t(p) = 1$, it follows that $u^t_{xx}(p) = u^t_{yy}(p) = 1/2$.

Let d_1, d_2, d_3 be vectors pointing from p to the vertices v_1, v_2, v_3 of the triangle as in Figure 5. By symmetry again, the gradient of u^t at any point of a median of the triangle is a multiple of d_j .

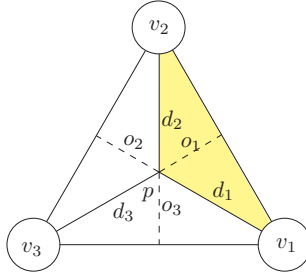


FIGURE 5. (Colour online) The equilateral triangular fundamental domain.

Assume, for the time being, that there is a δ such that for any given $t < \delta$ we have proven that $u_{d_j}^t(x) > 0$ at any x on the median joining p to the corresponding vertex (excluding the centre), i.e. along the medians the gradient points towards the vertices.

Under this assumption, we concentrate our attention on the yellow region in the picture consisting of one-third of the original domain Ω_t bounded by two of the medians. We will prove that on the yellow region the function $u_{o_1}^t$, which is the derivative of u^t in the direction $o_1 := -d_3$, is strictly positive. This is clear because the function $u_{o_1}^t$ is a harmonic function ($\Delta u_{o_1}^t = 0$) and on the boundary of the shaded region it is positive: On the medians it is positive by assumption, on the remaining side of the triangle it is actually 0 by the definition of u^t , and on the arcs of circles the gradient of u^t points towards the centre of the disks ($u^t \equiv 0$ on the boundary of the disks and it is negative in Ω_t), thus $u_{o_1}^t$ is positive on the arcs of circles that bound the shaded region.

Now any point q belonging to the yellow region has the property that $u(p) < u(q)$ since we can follow a path from p to q consisting of a line segment parallel to the median followed by a line segment in the direction of o_1 , and on both segments u^t will be increasing.

It remains to prove that $u_{d_j}^t(x) \geq 0$ on the corresponding median. Let us assume for the time being that this is the case for all $t \leq \delta$. We will prove then that this is true for all $t < t_0$.

Let us denote by t^* the largest t such that $u_{d_j}^t(x) \geq 0$ on all points of the median. Now we will see that if $t^* < t_0$, we reach a contradiction. By continuity, $u_{d_j}^{t^*}(x) \geq 0$ on the median. If we proved that actually

$$u_{d_j}^{t^*}(x) \geq c > 0 \quad (6.1)$$

on the median, we would have reached a contradiction since t^* would not be maximal. We cannot prove (6.1) directly since $u_{d_j}^t(p) = 0$ but, in a neighbourhood of p , $u_{d_j}^t(x) > u_{d_j}^t(p)$ since $u_{d_j}^t(p) = 1/2$. Thus, if t^* is maximal, it may only be for two reasons. Either there is a point q in the interior of the median different from p such that $u_{d_j}^{t^*}(q) = 0$ or the same thing happens for the point q' that is at the intersection of the median with the boundary of Ω_t . Let us examine these two cases separately. In the first case, $u_{d_j}^{t^*} \geq 0$ along the median but it vanishes in some intermediate position. By symmetry, this will happen in $u_{d_1}^{t^*}$ and $u_{d_2}^{t^*}$ simultaneously. Thus, $u_{o_1}^{t^*}$ is a harmonic function in the yellow region that is positive on the boundary (and strictly positive at some points on the boundary, for

instance near p). Thus, by the maximum principle, it is a strictly positive function in the interior of the yellow region. Thus, $u_{o_1}^*$ is positive on the median that bisects the yellow region. By symmetry again $u_{o_3}^*$ is positive on the segment of the median denoted by o_3 in the picture. Therefore, finally, $u_{d_1}^* \geq 0$ on the region bounded by o_1, o_3 and $\partial\Omega_t$. Finally, since $u_{d_1}^*$ is harmonic, it follows that it is strictly positive on the interior, i.e. on the median d_1 . Thus, such a point q does not exist.

On the other hand, $u_{d_1}^*$ cannot vanish at the endpoint e where the median d_1 meets the circle because we are assuming that $t^* < t_0$ and therefore the expected lifetime near the boundary of the disk can be estimated from below by the expected lifetime of a corona around the disk. This has an explicit expression that has positive derivative on the boundary. Thus, $u_{d_1}^*(e) > 0$. We have reached a contradiction.

It only remains to prove that we can start the argument, i.e. that there is a δ such that for any given $t < \delta$ we have that $u_{d_j}^t(x) > 0$ at any point x (excluding the centre) on the median joining p to a vertex. This is the case when $t = 0$. In this case we define $u^0 = v$, the Green's function. In this case, the gradient v_{d_j} is positive along each median because, by the results of [7], p is a unique critical point of v in the interior of Ω_0 . For very small t , the Green's function v has values in the circles around the vertices of the triangle very close to a constant. Thus, u^t can be obtained by adding to v a harmonic function that almost coincides with a constant in the circles. One can check that $u_{d_j}^t$ is close to v_{d_j} , and thus it is positive if t is small enough. \square

7 Conclusions

Complex analysis methods, and elliptic functions in particular, are used to estimate the maximum value, in absolute terms, of the solution to the boundary value problem $\Delta u = 1$ with zero Dirichlet boundary conditions in the complement of an infinite grid of disks of fixed size ε . This models the maximum voltage drop between power distribution pads in modern IC computer chips. The goal, building on existing work in the literature, is to compare different geometric arrangements of power pads with a view to minimizing the maximum voltage drop. With the normalisation that the areal density of pads is the same in all cases, it is found that an equilateral triangular power pad disposition outperforms the industry-dominant square power pad disposition. A hexagonal power pad disposition is also analysed and found to underperform both triangular and square arrangements. Other regular configurations of pads can be considered, but we do expect that the equilateral lattice is optimal. This is reminiscent of the Abrikosov conjecture, where it is speculated that free electrons under a uniform external magnetic field minimize their energy in an equilateral lattice. It has been recently proved, see [8], that among regular lattices the triangular one is optimal for the Abrikosov problem.

These mathematical results complement the work of Aquareles *et al.* [2], and are in agreement with the findings of Shakeri and Meindl [9] and Chen *et al.* [3] as well as with physical and SPICE models. We obtain simple explicit formulas for the maximum voltage drop in each of the power pad arrangements (square, triangular and hexagonal) as a function of the pad size ε . Finally, we establish rigorously that the maximum voltage

drop in the case of square or triangular grid arrangement occurs at the centre of a square or triangle respectively.

Acknowledgements

T. Carroll is supported by the UCC Strategic Research Fund 2012. J. Ortega-Cerdà is supported by the project MTM2011-27932-C02-01 and the CIRIT grant 2009SGR-1303. We wish to thank both referees for their careful reading of this paper and their many helpful comments and corrections.

References

- [1] ABRAMOWITZ, M. AND STEGUN, I. A. (eds.) (1992) *Handbook of Mathematical Functions with Formulas, Graphs, and Mathematical Tables*, Dover, New York, NY, xiv+1046 pp (reprint of the 1972 edition).
- [2] AGUARELES, M., HARO, J., RIUS, J. AND J. SOLÀ-MORALES (2012) On an asymptotic formula for the maximum voltage drop in a on-chip power distribution network. *Euro. J. Appl. Math.* **23**(2), 245–265.
- [3] CHEN, H., CHENG, C.-K., KAHNG, A. B., MANDOIU, I., WANG, Q. AND YAO, B. (2003) The Y-architecture for on-chip interconnect: Analysis and methodology. In: *Proceedings of the 2003 IEEE/ACM International Conference on Computer-Aided Design*, 9–13 November, 13 pp.
- [4] GRÖCHENIG, K. AND LYUBARSKII, Y. (2009) Gabor (super) frames with Hermite functions. *Math. Ann.* **345**, 267–286.
- [5] HAYMAN, W. K. (1974) The local growth of the power series: A survey of the Wiman-Valiron method. *Canad. Math. Bull.* **17**(3), 317–358 .
- [6] HILLE, E. (1949) *Analytic Function Theory*, Ginn and Co., Oxford, UK.
- [7] LIN, C.-S. AND CHIN-LUNG, W. (2010) Elliptic functions, Green functions and the mean field equations on tori. *Ann. Math.* **172**(2), 911–954.
- [8] SANDIER, E. AND SERFATY, S. (2012) From the Ginzburg–Landau Model to vortex lattice problems. *Comm. Math. Phys.* **313**, 635–743.
- [9] SHAKERI, K. AND MEINDL, J. D. (2005) Compact physical IR-drop models for chip/package co-design of gigascale integration (GSI). *IEEE Trans. Electron Devices* **52**(6), 1087–1096.